which extend their foot processes around the arterioles and capillaries, could be clearly identified (Figure 1D, arrows), and pericytes, which wrap around the capillaries, could also be clearly observed (Figure 1D, arrowheads). Plasma labeling with SR101 allowed us to visualize erythrocytes, which were detected as nonfluorescent particles within the plasma stream. The kinetics of erythrocytes in microcirculation could be detected dynamically by repeated volume scanning (Movie I in the online-only Data Supplement).

Regional CBF Under Chronic Cerebral Hypoperfusion

Figure 2 shows the mean CBF values, as measured by laser speckle flowmetry, in the both sham and BCAS groups (Figure 2A). In the sham group, CBF was not changed significantly throughout the entire observation period. In contrast, CBF values after the BCAS operation were significantly decreased when compared with those of preoperative baselines and sham controls (Figure 2B).

Figure 3 shows the inflow (pial artery) and outflow (pial vein) velocity changes in the 2 groups. Specifically, we measured the slope of line scan images of pial arteries (Figure 3A) and veins (Figure 3B) to indicate inflow and outflow velocity, respectively, at each time point.[12] In the sham group, inflow velocity was not changed significantly throughout the entire observation period. In contrast, the inflow velocity after BCAS operation was significantly decreased when compared with those of preoperative baselines and sham controls (Figure 3C). Similarly, outflow velocity was not changed in the sham group, and significantly decreased after BCAS operation when compared with those of preoperative baselines and sham controls (Figure 3D).

Anatomic Morphology Under Chronic Cerebral Hypoperfusion

Under chronic cerebral hypoperfusion, the small pial vessels and the deep cortical capillaries did not show obvious morphological changes such as vascular loss or angiogenesis throughout the entire observation period (Figure 4A). Vascular shape such

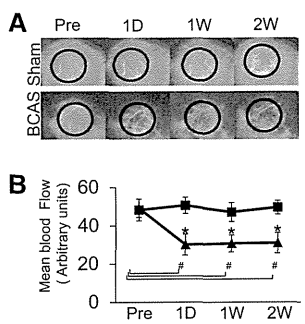

Figure 2. Temporal profile of cerebral blood flow (CBF) in the sham-operated and bilateral common carotid artery stenosis (BCAS) mice. Mean CBF was analyzed by laser speckle flowmetry through the same cranial window as was used for 2-photon laser-scanning. The circle indicates the cranial window. **A**, CBF changes in the sham and BCAS group. The line graph (**B**) indicates CBF changes in the sham (■) and BCAS (▲) groups. Data are presented as mean±SD. *P<0.05 vs sham value. #P<0.05 between different time points. 1D indicates 1 day; 1W, 1 week; and 2W, 2 weeks.

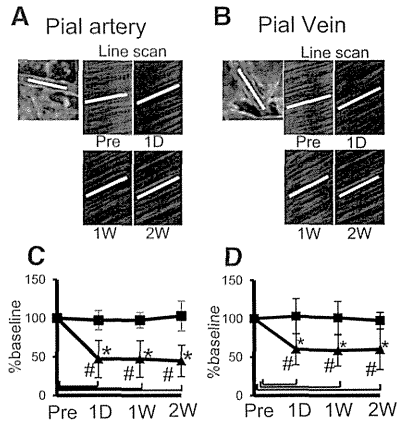

Figure 3. Inflow velocity of the pial arteries and outflow velocity of the pial veins analyzed by repetitive line-scans. **A**, Inflow velocity of the pial artery. The white line in a reference image indicates the central longitudinal axis of a selected small pial artery. Slopes of the lines in line-scan images indicate the inflow velocity. Line graphs (**C**) indicate arterial inflow changes in the sham (■) and bilateral common carotid artery stenosis (BCAS; ▲) groups. **B**, Outflow velocity of the pial vein. The line in a reference image indicates the central longitudinal axis of a selected small pial vein. Slopes of the lines in line-scan images indicate the outflow velocity. Line graphs (**D**) indicate venous outflow changes in the sham (■) and BCAS (▲) groups. Data are presented as mean±SD. *P<0.05 vs sham value. #P<0.05 between different time points. 1D indicates 1 day; 1W, 1 week; and 2W, 2 weeks.

as tortuosity and size for arterioles (Figure 4B) and venules was not changed throughout the observation period, and obvious changes of wall thickness for arterioles (Figure 4B, Lt lower inset) and venules were also not detected. Although the arteriolar lumen (Figure 4B, Rt lower inset) slightly increased in post-BCAS operation, there was no significant difference in luminal area over time (1 day, 119.9±49.5%; 1 week, 102.2±14.1%; 2 weeks, 104.9±23.3% compared with the preoperative baseline). The venular lumen in the BCAS group also remained unchanged throughout the entire observation period (1 day, 95.2±12.5%; 1 week , 95±12.4%; 2 weeks, 106.6±15.1% compared with the preoperative baseline). In the sham group, wall thickness and luminal area did not show obvious changes throughout the observation period. Figure 4C show that astrocytes extended their foot process around the vessels but showed no obvious morphological differences between pre- and post-BCAS operative periods. In addition, pericytes were found to wrap around capillaries at the both periods with no morphological changes. Taken together, astrocytes and pericytes remained unchanged morphologically between BCAS and sham groups during the entire observation period.

Microcirculation in Deep Cortical Capillaries Under Chronic Cerebral Hypoperfusion

Figure 5A and Movies II to V in the online-only Data Supplement show representative microcirculation in the deep cortical capillaries under chronic cerebral hypoperfusion. Under low magnification, stagnation of capillary flow, which was detected as high fluorescent plasma segments without nonfluorescent erythrocytes (Figure 5A, white arrows; Movie III, in the online-only Data Supplement), was observed under chronic cerebral hypoperfusion, whereas it was rarely found under

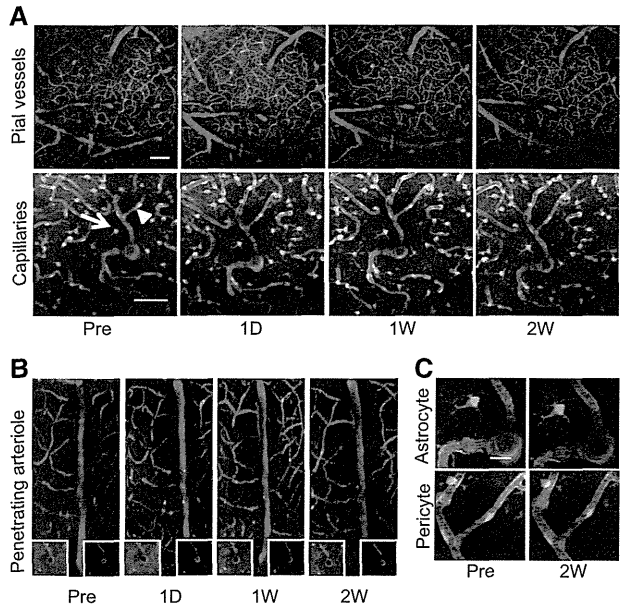

Figure 4. Two-photon images of the pial microvasculature (maximum intensity projection [MIP] from the surface of the brain to 100-μm depth) and the deep cortical capillaries (MIP from 300–350-μm depth) with green fluorescent protein (GFP) and SR101 fluorescence in the bilateral common carotid artery stenosis (BCAS) group for each time point (**A**). Scale bar in the upper column, 100 μm. Scale bar in the lower column, 30 μm. Three-dimensional (3D) reconstruction for penetrating arterioles at each time point (**B**). Lt lower inset in **B** indicates single plane zoom images for the vessel walls in the volume of interest (VOI) of an artery with GFP fluorescence; Rt lower inset in **B** indicates single plane zoom images for the vessel lumens in the VOI of the artery. **C**, The zoomed images of astrocyte (arrow in **A**) and pericyte (arrowhead in **A**) at the preoperative period and 2 weeks after BCAS operation. Scale bar, 10 μm. 1D indicates 1 day; 1W, 1 week; and 2W, 2 weeks.

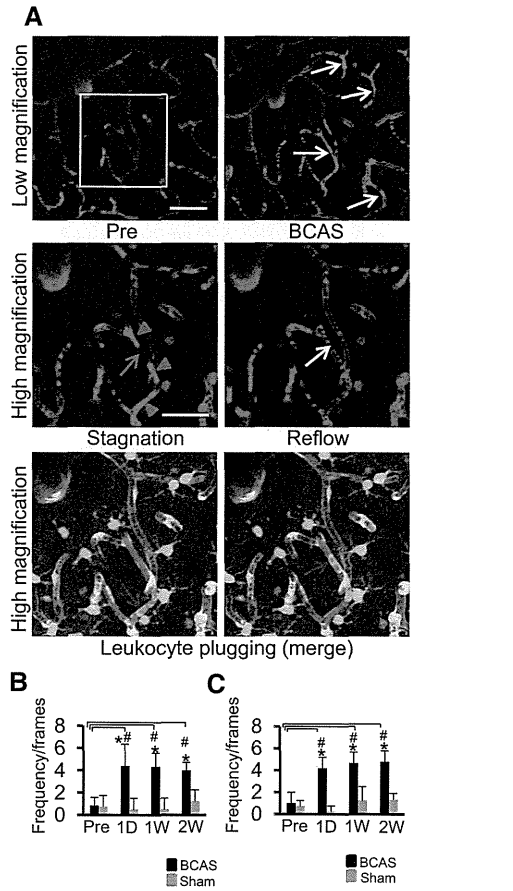

Figure 5. Microcirculation of the deep cortical capillaries in the volume of interest (VOI) of a vein (250–300-μm depth). Upper column in **A** denotes plasma labeling images with SR101 during the preoperative normal period and at follow-up periods 2 weeks after bilateral common carotid artery stenosis operations. The white arrow indicates the stagnation of capillary flow. Scale bar, 30 μm. Middle column denote zoom images (rectangle in upper column) with capillary plugging (blue arrow) and with reflow after the plug was released (yellow arrow) 2 weeks after the operation. Blue arrowheads indicate high fluorescent capillary plasma without erythrocytes. Scale bar, 30 μm. Lower column denotes the merged green fluorescent protein (GFP; green) and SR101 (red) image. Purple arrows indicate the single pulling leukocyte as GFP-positive (100-s interval). Bar graphs indicate the frequency of stagnation of capillary flow in the VOI of arteries (**B**) and the VOI of veins (**C**) in each group. Data are presented as mean±SD. *P<0.05 vs sham values. #P<0.05 between different time points. 1D indicates 1 day; 1W, 1 week; and 2W, 2 weeks.

normal microcirculation (Movie II in the online-only Data Supplement). We also observed leukocyte plugging (Figure 5A, blue arrow) in the high fluorescent plasma stagnated capillary (Figure 5A, blue arrowheads) under higher magnification (Movies IV and V in the online-only Data Supplement). Plugged leukocytes did not tightly obstruct capillaries, but slowly moved downstream (Figure 5A, purple arrows) and eventually were released (plugging time was usually <120 s), resulting in reflow of plasma streams with erythrocytes (Figure 5A, yellow arrow). Long-term and complete leukocyte plugging, as well as leukocyte infiltration, in the perivascular parenchyma could not be identified during the observation period. On the contrary, platelet activation (Methods and Figure III in the online-only Data Supplement), which is a pivotal mechanism of focal cerebral ischemia, could not be found during the observation period. Frequency of capillary flow stagnation in the BCAS group was markedly higher than that of the sham group throughout the entire observation period (Figure 5B and 5C).

Leukocyte Rolling and Adhesion in the Cortical Vessels Under Chronic Cerebral Hypoperfusion

In the sham-operated group, rolling and adhesion were rarely detected throughout the entire observation period (Figure 6A). After BCAS operation, however, rolling and adhesion of leukocytes were typically observed in the pial venules although rarely in the pial arterioles under chronic cerebral hypoperfusion (Figure 6A, arrows). From 1 day to 2 weeks after the BCAS operation, the frequency of rolling and adherent leukocytes decreased in the both small pial veins and pial arteries (Figure 6B and 6C). However, 2 weeks after BCAS operation, the frequency of rolling and adhesion was still higher significantly in the pial veins.

Discussion

Neuron-targeted therapies against brain ischemia have been uniformly unsuccessful in clinical trials. This is thought to be a consequence of lack of understanding of the integrated response among neuronal, glial, and vascular elements.[1–5] Each of these elements responds to an ischemic event by activation

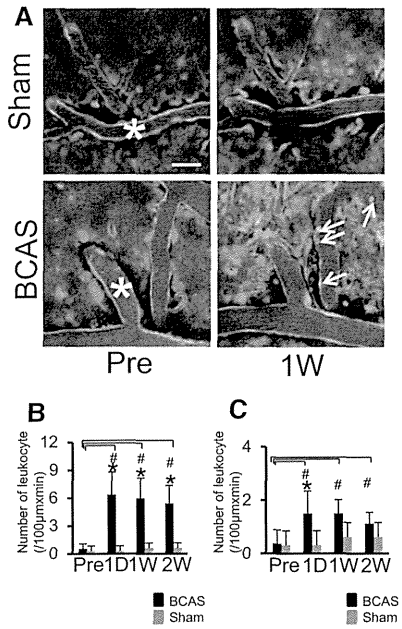

Figure 6. Two-photon images of leukocyte rolling and adhesion in the small pial arteries and veins. **A**, A pial artery (*) and vein (※) for each group in different time points. The arrows indicate rolling and adhesion of leukocytes. Scale bar, 30 μm. Bar graphs indicate the frequency of rolling and adhesion of leukocytes in the pial veins (**B**) and in the pial arteries (**C**). Data are presented as mean±SD. *P<0.05 vs sham values. #P<0.05 between different time points. 1D indicates 1 day; 1W, 1 week; and 2W, 2 weeks.

and individual features of specific cell responses are well studied, but it remains unknown how they respond as a NVU.[13] In this study, we developed an in vivo imaging method for the NVU. This method allows repeated longitudinal observation of the NVU in 3D, which is helpful to understand anatomic morphology of microvessels with varying sizes as a whole. In addition, this method allows identification of cellular components (astrocytes, pericytes, circulating leukocytes, and platelets) and allows investigation of the anatomic relationship between these cells. This imaging approach also provides semiquantitative information on the kinetics of erythrocytes and leukocytes to understand microcirculation alteration.

Chronic cerebral hypoperfusion induces subcortical white matter lesions and vascular cognitive impairment. This condition is often an initial trigger of a cascade of pathophysiological changes in the NVU[2–4] and can be experimentally replicated in animal models of chronic cerebral hypoperfusion such as BCAS model.[9,14] In these models, gray matter exhibits more slight pathophysiological changes than white matter under chronic cerebral hypoperfusion. In this study, we could not detect any morphological change in the cortical gray matter. The morphological changes as stress response of NVU in the cerebral cortex may be limited and under the detection level of 2-photon laser microscopy method. However, additional studies will be required to address this point finally.

As for the dynamic microcirculation, there was stagnation of capillary flow and plugging by leukocytes under chronic cerebral hypoperfusion. The phenomenon of capillary plugging has been postulated to explain no-reflow phenomenon during early reperfusion after ischemia.[15,16] After several hours of ischemia, an incomplete restoration of blood flow, no-reflow phenomenon, has been reported also in other organs.[17–19] Many pathophysiological mechanisms have been implicated in this process, however, the exact mechanisms responsible for this phenomenon have been unclear. Leukocytes are large stiff cells, which physiologically adhere to vascular endothelium, and are known to express adhesion molecules under a variety of conditions.[20] The present study has provided the first evidence that leukocyte transiently plugs capillaries under chronic cerebral hypoperfusion, and this plugging has induced stagnation of capillary flow. In this stagnated plasma, no oxygen-transporting erythrocytes were found, implying a viscous cycle for further exacerbation of parenchymal hypoxia. On the contrary, platelet activation was not observed throughout the observation period. Antiplatelet treatment has been the target of therapeutic strategies for chronic cerebral hypoperfusion, but this strategy should be substituted for the agents that have the potential to suppress plugging of leukocytes and restore insufficient CBF. Indeed, beneficial effect of induced immune tolerance against adhesion molecules has been revealed in chronic cerebral hypoperfusion previously.[21]

Leukocyte rolling and adhesion in the pial vessels have been reported in various organs under a variety of conditions, appearing more prominently in the venules than in the arterioles.[22–24] In accordance with these observations, leukocyte rolling and adhesion were observed typically in the pial veins during chronic cerebral hypoperfusion. Our results may further indicate that leukocyte activation may be the first step eventually leading to stress response of the whole NVU to chronic cerebral hypoperfusion.

Conclusions

In this study, we established an in vivo imaging method for the NVU and provided evidence that leukocytes activation may play a critical role in microcirculation disturbance under chronic cerebral hypoperfusion.

Acknowledgments

The study was conceived by Dr Tomimoto, and the protocol was drafted by Drs Suzuki, Tanaka, Mizoguchi, and Tomimoto. Drs Yata, Nishimura, Unekawa, and Tomita performed the experiments. Dr Yata was responsible for data analysis, data interpretation, and preparation of the report. All authors contributed to data interpretation and approved the final version.

Sources of Funding

This work was supported by Grants-in-Aid for Scientific Research (KAKENHI) grant number 22590929.

Disclosures

None.

References

1. Lo EH, Dalkara T, Moskowitz MA. Mechanisms, challenges and opportunities in stroke. *Nat Rev Neurosci.* 2003;4:399–415.
2. Stanimirovic DB, Friedman A. Pathophysiology of the neurovascular unit: disease cause or consequence? *J Cereb Blood Flow Metab.* 2012;32:1207–1221.
3. del Zoppo GJ. Aging and the neurovascular unit. *Ann N Y Acad Sci.* 2012;1268:127–133.

4. Dirnagl U. Pathobiology of injury after stroke: the neurovascular unit and beyond. *Ann N Y Acad Sci*. 2012;1268:21–25.
5. Zhang L, Zhang ZG, Chopp M. The neurovascular unit and combination treatment strategies for stroke. *Trends Pharmacol Sci*. 2012;33:415–422.
6. Okabe M, Ikawa M, Kominami K, Nakanishi T, Nishimune Y. 'Green mice' as a source of ubiquitous green cells. *FEBS Lett*. 1997;407:313–319.
7. Tomita Y, Kubis N, Calando Y, Tran Dinh A, Méric P, Seylaz J, et al. Long-term in vivo investigation of mouse cerebral microcirculation by fluorescence confocal microscopy in the area of focal ischemia. *J Cereb Blood Flow Metab*. 2005;25:858–867.
8. Masamoto K, Tomita Y, Toriumi H, Aoki I, Unekawa M, Takuwa H, et al. Repeated longitudinal in vivo imaging of neuro-glio-vascular unit at the peripheral boundary of ischemia in mouse cerebral cortex. *Neuroscience*. 2012;212:190–200.
9. Shibata M, Ohtani R, Ihara M, Tomimoto H. White matter lesions and glial activation in a novel mouse model of chronic cerebral hypoperfusion. *Stroke*. 2004;35:2598–2603.
10. Tsukuda K, Mogi M, Li JM, Iwanami J, Min LJ, Sakata A, et al. Diabetes-associated cognitive impairment is improved by a calcium channel blocker, nifedipine. *Hypertension*. 2008;51:528–533.
11. Fernández-Klett F, Offenhauser N, Dirnagl U, Priller J, Lindauer U. Pericytes in capillaries are contractile in vivo, but arterioles mediate functional hyperemia in the mouse brain. *Proc Natl Acad Sci U S A*. 2010;107:22290–22295.
12. Nimmagadda A, Park HP, Prado R, Ginsberg MD. Albumin therapy improves local vascular dynamics in a rat model of primary microvascular thrombosis: a two-photon laser-scanning microscopy study. *Stroke*. 2008;39:198–204.
13. Moskowitz MA, Lo EH, Iadecola C. The science of stroke: mechanisms in search of treatments. *Neuron*. 2010;67:181–198.
14. Tomimoto H, Wakita H. Animal models of vascular dementia: translational potential at present and in 2050. *Future Neurology*. 2014;9:163–172.
15. Grøgaard B, Schürer L, Gerdin B, Arfors KE. Delayed hypoperfusion after incomplete forebrain ischemia in the rat. The role of polymorphonuclear leukocytes. *J Cereb Blood Flow Metab*. 1989;9:500–505.
16. del Zoppo GJ, Schmid-Schönbein GW, Mori E, Copeland BR, Chang CM. Polymorphonuclear leukocytes occlude capillaries following middle cerebral artery occlusion and reperfusion in baboons. *Stroke*. 1991;22:1276–1283.
17. Helmke BP, Bremner SN, Zweifach BW, Skalak R, Schmid-Schönbein GW. Mechanisms for increased blood flow resistance due to leukocytes. *Am J Physiol*. 1997;273(6 pt 2):H2884–H2890.
18. Fukuda S, Yasu T, Kobayashi N, Ikeda N, Schmid-Schönbein GW. Contribution of fluid shear response in leukocytes to hemodynamic resistance in the spontaneously hypertensive rat. *Circ Res*. 2004;95:100–108.
19. Salinas P, Jimenez-Valero S, Moreno R, Sanchez-Recalde A, Galeote G, Calvo L, et al. Update in pharmacological management of coronary no-reflow phenomenon. *Cardiovasc Hematol Agents Med Chem*. 2012;10:256–264.
20. Yilmaz G, Granger DN. Leukocyte recruitment and ischemic brain injury. *Neuromolecular Med*. 2010;12:193–204.
21. Wakita H, Ruetzler C, Illoh KO, Chen Y, Takanohashi A, Spatz M, Hallenbeck JM. Mucosal tolerization to E-selectin protects against memory dysfunction and white matter damage in a vascular cognitive impairment model. *J Cereb Blood Flow Metab*. 2008;28:341–353.
22. Uhl E, Beck J, Stummer W, Lehmberg J, Baethmann A. Leukocyte-endothelium interactions in pial venules during the early and late reperfusion period after global cerebral ischemia in gerbils. *J Cereb Blood Flow Metab*. 2000;20:979–987.
23. Ishikawa M, Cooper D, Arumugam TV, Zhang JH, Nanda A, Granger DN. Platelet-leukocyte-endothelial cell interactions after middle cerebral artery occlusion and reperfusion. *J Cereb Blood Flow Metab*. 2004;24:907–915.
24. Kataoka H, Kim SW, Plesnila N. Leukocyte-endothelium interactions during permanent focal cerebral ischemia in mice. *J Cereb Blood Flow Metab*. 2004;24:668–676.

Water diffusion reveals networks that modulate multiregional morphological plasticity after repetitive brain stimulation

Mitsunari Abe[a,b,c,1], Hidenao Fukuyama[a], and Tatsuya Mima[a,1]

[a]Human Brain Research Center, Kyoto University Graduate School of Medicine, Kyoto 606-8501, Japan; [b]Department of Functional Brain Research, National Institute of Neuroscience, National Center of Neurology and Psychiatry, Tokyo 187-8502, Japan; and [c]Department of Neurology, Fukushima Medical University, Fukushima 960-1295, Japan

Edited by Marcus E. Raichle, Washington University, St. Louis, MO, and approved February 14, 2014 (received for review October 29, 2013)

Repetitive brain stimulation protocols induce plasticity in the stimulated site in brain slice models. Recent evidence from network models has indicated that additional plasticity-related changes occur in nonstimulated remote regions. Despite increasing use of brain stimulation protocols in experimental and clinical settings, the neural substrates underlying the additional effects in remote regions are unknown. Diffusion-weighted MRI (DWI) probes water diffusion and can be used to estimate morphological changes in cortical tissue that occur with the induction of plasticity. Using DWI techniques, we estimated morphological changes induced by application of repetitive transcranial magnetic stimulation (rTMS) over the left primary motor cortex (M1). We found that rTMS altered water diffusion in multiple regions including the left M1. Notably, the change in water diffusion was retained longest in the left M1 and remote regions that had a correlation of baseline fluctuations in water diffusion before rTMS. We conclude that synchronization of water diffusion at rest between stimulated and remote regions ensures retention of rTMS-induced changes in water diffusion in remote regions. Synchronized fluctuations in the morphology of cortical microstructures between stimulated and remote regions might identify networks that allow retention of plasticity-related morphological changes in multiple regions after brain stimulation protocols. These results increase our understanding of the effects of brain stimulation-induced plasticity on multiregional brain networks. DWI techniques could provide a tool to evaluate treatment effects of brain stimulation protocols in patients with brain disorders.

Repetitive electrical brain stimulation induces long-term potentiation (LTP) or depression (LTD) at the stimulated neurons (1–4). In humans, repetitive transcranial magnetic stimulation (rTMS) alters cortical excitability at the stimulated site that outlasts the end of the stimulation, analogous to LTP or LTD in animal models (5, 6), but also affects remote regions, possibly through transsynaptic pathways (7, 8). Although rTMS has been proposed as a potential treatment for neurological and psychiatric disorders (9, 10) and as a method to facilitate learning (11), the neural substrates underlying the effects of rTMS on remote regions of the brain remain poorly understood.

Diffusion-weighted MRI (DWI) probes water diffusion, a thermal physical phenomena that is characterized by random motion of water molecules (12). Water diffusion is altered by the structures of gray matter (12). DWI can be used to evaluate morphological changes in cortical microstructures (13–19) and can function as a probe to estimate immediate and transient changes in water diffusion that are associated with ischemia (17) or neuronal firing (13, 16, 19) and delayed and persistent changes that are associated with long-term plasticity in experimental settings (20) or pathological conditions (15, 18, 21). Here, using DWI techniques, we examined whether subthreshold, low-frequency (<1 Hz) rTMS to the left primary motor cortex (M1), a protocol that induces LTD-like plasticity (22, 23), increased water diffusion in the left M1 and other regions after the end of rTMS. Because it can be assumed that the motion of water molecules is not restricted to particular directions, that is, water diffusion is not anisotropic within cortical tissue, we measured the DWI signals along a single direction (*Methods*), which enabled us to extrapolate mean water diffusion in gray matter in the sampled direction (16). We did not measure anisotropic water diffusion with respect to particular directions to estimate white matter microstructure (12). We used the MRI-compatible TMS and EMG system that was developed (24) to measure mean water diffusion and estimate LTD-like plasticity inside the bore of an MRI scanner (see *Methods* for the detailed procedures).

Results

Subthreshold, low-frequency rTMS was applied to the hand area of the left M1 for 10 min using an established protocol to induce LTD-like plasticity (23) (Fig. 1). To assess the corticospinal stimulus-response function, the amplitude of motor-evoked potentials (MEPs) was measured before rTMS (baseline) and immediately, 10 min, and 20 min after rTMS (5, 6, 25). MEP amplitude immediately after rTMS was lower than at baseline but recovered to baseline levels by 10 min after rTMS (Fig. S1), confirming that the rTMS protocol induced a transient LTD-like plasticity in the left M1.

DWI was performed with high and low b values (b = 1,200 and 300 s/mm^2, respectively) during periods of rest when the subject

Significance

Repetitive brain stimulation is an established experimental protocol that induces plasticity in the stimulated site. Recent evidence indicates additional plasticity-related changes in remote nonstimulated regions. However, the neural substrates underlying the remote effects are unknown. Diffusion-weighted MRI (DWI) probes water diffusion and can be used to estimate morphological changes in cortical tissue that occur with the induction of plasticity. We used DWI to evaluate morphological changes induced by repetitive brain stimulation in human brains. Our results reveal that synchronized fluctuations in the morphology of microstructures between stimulated and remote regions might form identify networks that allow retention of plasticity-related morphological changes in remote regions. These results increase our understanding of the effects of stimulation-induced plasticity on multiple brain regions.

Author contributions: M.A., H.F., and T.M. designed research; M.A. and T.M. performed research; M.A. contributed new reagents/analytic tools; M.A. and T.M. analyzed data; and M.A., H.F., and T.M. wrote the paper.

The authors declare no conflict of interest.

This article is a PNAS Direct Submission.

Freely available online through the PNAS open access option.

[1]To whom correspondence may be addressed. E-mail: mitzabe@gmail.com or mima@kuhp.kyoto-u.ac.jp.

This article contains supporting information online at www.pnas.org/lookup/suppl/doi:10.1073/pnas.1320223111/-/DCSupplemental.

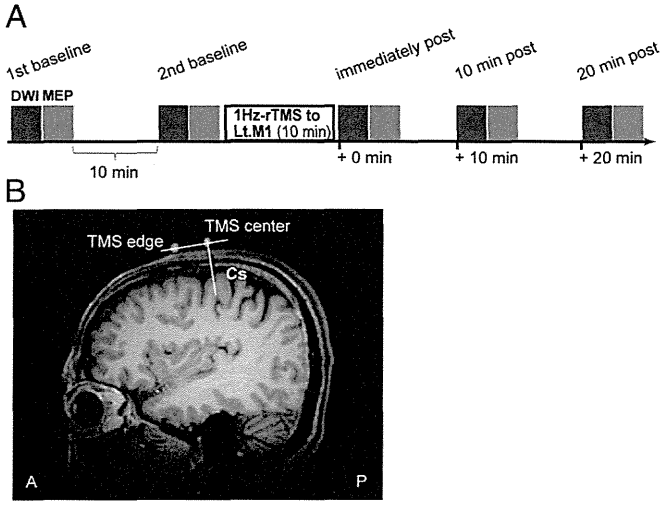

Fig. 1. Experimental procedures. (*A*) Experimental design. Subthreshold, 1-Hz rTMS was applied to the hand area of the left primary motor cortex for 10 min. The stimulation intensity was 90% of resting motor threshold and was not strong enough to induce contractions in the muscles of the right hand. DWI (blue bars) was performed with high (1,200 s/mm^2, n = 72 scans at each time point) and low (300 s/mm^2, n = 18 scans at each time point) b values, and MEPs (red bars, n = 20 at each time point) were measured at two baseline time points, and immediately, 10 min, and 20 min after rTMS. The two baseline measurements were separated by 10 min. Throughout the entire experiment, the subjects were inside an MRI scanner and were instructed to keep still with their eyes open. (*B*) The position of the TMS coil relative to the central sulcus (C_S) in one subject (T.A.). White dots indicate the positions of the center (TMS center) and edge (TMS edge) of the figure-eight-shaped coil. The line perpendicular to the line crossing these two dots passes through the hand area of the left primary motor cortex and indicates the optimal position of the coil for maximally stimulating this region.

was not engaged in any tasks (Fig. 1). Water diffusion was estimated from the DWI data acquired with a b value of 1,200 s/mm^2 (b1200 DWI) (14, 16), because these data were more sensitive to changes in intracortical water diffusion than data obtained with a b value of 300 s/mm^2 (Figs. S2 and S3).

Two baseline measurements were made, separated by 10 min. Water diffusion did not change between the two baseline time points in any region (uncorrected $P < 0.01$). At the immediately after rTMS time point, there was an increase in water diffusion in the left M1, left superior parietal lobule (SPL, area 5), left premotor cortex (PM), right PM, and supplementary motor area [SMA; cluster level of family-wise error (FWE)-corrected $P < 0.05$; Fig. 2 and Table 1]. The magnitude of the change in water diffusion was similar in all regions (one-way ANOVA, $P = 0.15$).

The change in water diffusion in the left M1 from baseline to immediately after rTMS was correlated with the change in water diffusion in the left SPL (simple regression, $t_{11} = 4.15$, $P = 0.007$, $R^2 = 0.64$) and the right PM ($t_{11} = 3.94$, $P = 0.01$, $R^2 = 0.62$), but not with the change in water diffusion in the left PM ($t_{11} = 1.31$, $P = 0.37$, $R^2 = 0.07$) or SMA ($t_{11} = 1.75$, $P = 0.22$, $R^2 = 0.11$; Fig. S4). A homogeneity test with ANCOVA in a factorial design with one factor [regions of interest except for left M1, $\text{REGION}_{(\text{left SPL/right PM/left PM/SMA})}$], one variable [water diffusion in REGION, $\text{WATER DIFFUSION}_{(\text{REGION})}$], and one covariate [water diffusion in left M1, $\text{WATER DIFFUSION}_{(\text{left M1})}$] showed a significant interaction between $\text{REGION}_{(\text{left SPL/right PM/left PM/SMA})}$ and $\text{WATER DIFFUSION}_{(\text{left M1})}$ [$F_{(3)} = 4.37$, $P = 0.009$], supporting the significantly different regression slopes observed when the left M1 was paired with the left SPL or right PM and when it was paired with the left PM or SMA (left $\text{SPL}_{\text{left M1}}$ vs. right $\text{PM}_{\text{left M1}}$, $P = 0.50$; left $\text{SPL}_{\text{left M1}}$ vs. left $\text{PM}_{\text{left M1}}$, $P < 0.001$; left $\text{SPL}_{\text{left M1}}$ vs. $\text{SMA}_{\text{left M1}}$, $P < 0.001$; right $\text{PM}_{\text{left M1}}$ vs. left $\text{PM}_{\text{left M1}}$, $P = 0.003$; right $\text{PM}_{\text{left M1}}$ vs. $\text{SMA}_{\text{left M1}}$, $P < 0.001$; left $\text{PM}_{\text{left M1}}$ vs. $\text{SMA}_{\text{left M1}}$, $P = 0.63$).

At 10 min after rTMS, the increase in water diffusion was retained in the left M1, left SPL, and right PM ($P = 0.001$ FWE, $P = 0.005$ FWE, and $P = 0.001$ FWE, respectively, relative to baseline and corrected within the search volume; *Methods*), with no change from the immediately after rTMS time point, even at a liberal threshold of uncorrected $P = 0.01$ (Fig. 3, *Upper*). The change from baseline in the left M1 remained correlated with the change from baseline in the left SPL ($t_{11} = 4.59$, $P = 0.001$, $R^2 = 0.66$) and the right PM ($t_{11} = 3.29$, $P = 0.01$, $R^2 = 0.58$; *SI* 4). In contrast, water diffusion in the left PM and SMA recovered to baseline levels (uncorrected $P < 0.05$; Fig. 3, *Lower*), and significantly decreased from immediately after to 10 min after rTMS ($P = 0.02$ FWE and $P = 0.04$ FWE corrected within the search volume for left PM and SMA, respectively). Within-subject comparisons showed that the post-rTMS change in water diffusion was retained longer in the left M1, left SPL, and right PM than in the left PM and SMA (*SI Text*). At 20 min after rTMS, the water diffusion was similar to baseline in all regions (voxel level of uncorrected $P < 0.05$).

To investigate the network property accountable for the multiregional rTMS-induced changes in water diffusion, we used simple regression analyses to test the baseline coherent correlation of the intrinsic fluctuations in water diffusion between the

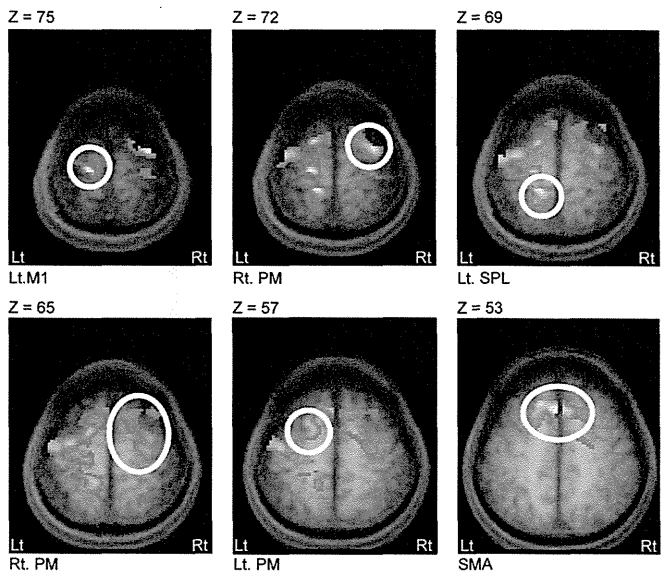

Fig. 2. The left M1 and remote regions of the brain showed a significant increase in water diffusion immediately after the end of rTMS. Images were acquired with an axial field of view covering the hand area of the left M1 and other motor-related regions that were affected by 1-Hz rTMS over the hand area of the left M1 (7, 8). Data acquired with a b value of 1200 s/mm^2 were used to estimate change in water diffusion (14, 16). Mean signal intensity was calculated for each voxel at each time point as the average of the 72 scans acquired with a b value of 1,200 s/mm^2 and was compared voxel-by-voxel between the baseline and the immediately post rTMS time points within subjects. The threshold was set to a cluster size of $P < 0.05$ corrected with a voxel-level threshold uncorrected $P < 0.005$. Results are overlaid on axial slices (Z = 75–53) of the averaged anatomical MRI brain. There was a decrease in mean signal intensity, indicating an increase in water diffusion, at the stimulated site (left M1), left SPL, left PM, right PM, and SMA. The coordinate of the peak signal intensity in each of these regions is shown in Table 1. Note that decreased signal intensity indicates increased water diffusion. The same results, i.e., increased water diffusion, were also obtained when the apparent diffusion coefficient was analyzed (Fig. S3). No significant change in water diffusion was observed in any region when data obtained using a lower b value (300 s/mm^2) were analyzed (Fig. S2).

Table 1. Brain regions showing increased water diffusion after the rTMS train

Brain region	Hemisphere	MNI coordinates of peak activation			t value of peak activation
		x	y	z	
Primary motor cortex	Left	−16	−23	75	7.68
Premotor cortex	Right	30	−17	65	6.29
Supplementary motor area	Left	−2	17	53	5.90
Superior parietal lobule	Left	−16	−39	69	5.83
Premotor cortex	Left	−20	7	53	4.96

Data represent peak t values in significant clusters and their coordinates.

left M1 and each remote region (Fig. 4*A*). The left M1 had a significant correlation with the right PM ($R^2 = 0.37 \pm 0.01$, $P < 0.001$) and the left SPL ($R^2 = 0.18 \pm 0.01$, $P < 0.001$) compared with the null distribution computed with a resampled bootstrap procedure (*Methods*). The left M1 did not have a significant correlation with the left PM or SMA (left PM, $R^2 = 0.05 \pm 0.02$, $P = 0.15$; SMA, $R^2 = 0.008 \pm 0.003$, $P = 0.60$), but the left PM and the left SMA had a correlation with each other ($R^2 = 0.42 \pm 0.02$, $P < 0.001$). The left M1 had a stronger correlation with the right PM and the left SPL than with the left PM or SMA (right PM vs. left PM, $P < 0.001$; right PM vs. SMA, $P < 0.001$; left SPL vs. left PM, $P < 0.001$; left SPL vs. SMA, $P < 0.001$; Fig. 4*B*). Neither the strength of the coherent correlation or the slope predicted the size of the rTMS-induced change in water diffusion in any of the remote regions ($P > 0.5$). Coherency or slope of the regression analysis did not change after rTMS in any of the pairs between the left M1 and a remote region ($P > 0.5$).

Discussion

In summary, a 10-min-long period of subthreshold 1-Hz rTMS produced LTD-like plasticity in the left M1 and a multiregional increase in water diffusion in the left M1, left PM, left SPL, right PM, and SMA immediately after the end of the simulation. The baseline fluctuations in water diffusion in the left M1 were synchronized with those in the left SPL and the right PM, but not with those in the left PM or the SMA. The left M1, left SPL, and right PM retained the change in water diffusion for 10 min after the end of rTMS, and the magnitude of the rTMS-induced change in water diffusion in the left M1 was correlated with that in the left SPL and the right PM. In contrast, the regions in which baseline

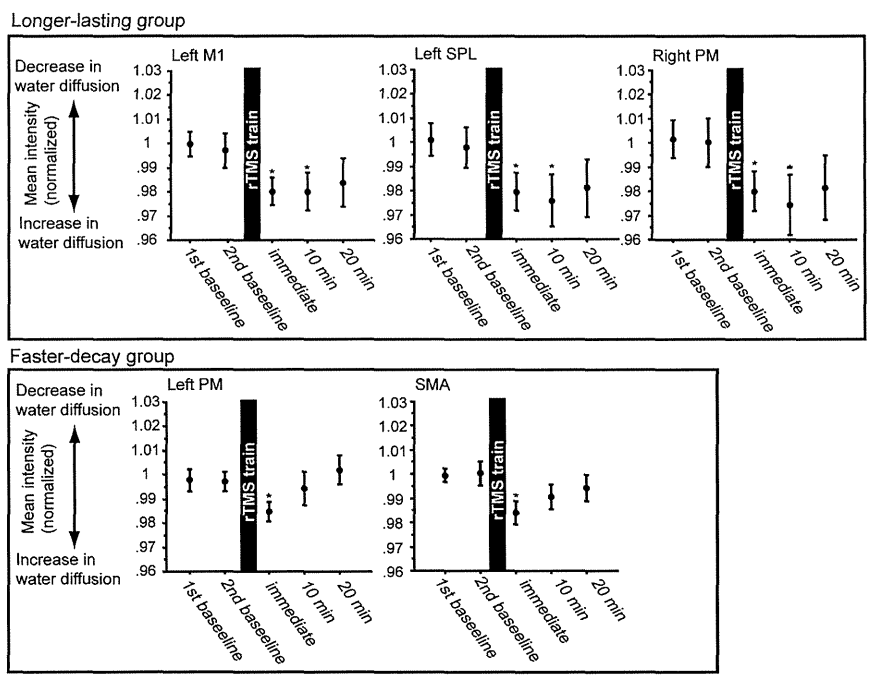

Fig. 3. The rTMS-induced change in water diffusion was sustained for a longer period in the left M1, left SPL, and right PM than in the left PM or SMA. The mean normalized signal intensity in each brain region at each time point. The mean intensity was calculated as the mean of the voxels within a 10-mm sphere centered at the coordinate of the peak signal intensity in the region of interest (Table 1) and was normalized for each subject (*Methods*). The mean signal intensity at the 10- and 20-min after rTMS time points was compared with the baseline and immediately after rTMS time points within each region of interest using statistical parametric maps. The threshold was FWE corrected within the search volume (*Methods*). Asterisks indicate significant difference ($P < 0.05$) in the signal intensity compared with the baseline sessions. Bars indicate SEM. Note that decreased signal intensity indicates increased water diffusion and increased signal intensity indicates decreased water diffusion. The mean signal intensity was lower (i.e., water diffusion was higher) immediately after rTMS than at baseline in the left M1 and other regions (Fig. 2 and Table 1). At 10 min after rTMS, the decrease was sustained in the left M1, left SPL, and right PM (*Upper*) but was not sustained in the left PM or the SMA (*Lower*). At 20 min after rTMS, water diffusion had returned to baseline values in all regions (no difference even at a liberal threshold of uncorrected $P = 0.1$). At the 10- and 20-min after time points, no additional regions (i.e., regions additional to those identified at the immediately post time point) showed a significant change in the mean signal intensity.

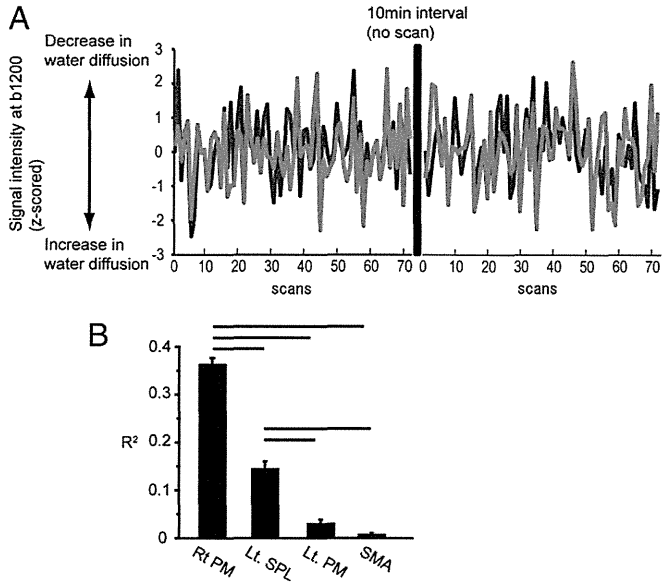

Fig. 4. Baseline fluctuations in water diffusion in the left M1 were coupled with fluctuations in water diffusion in the right PM and the left SPL more tightly than they were coupled with fluctuations in the left PM or SMA. (*A*) Water diffusion in the left M1 and right PM in each of the 144 scans from the two baseline time points in a representative subject. Data were transformed to z scores within each measurement time point (*Methods*). (*B*) R^2 was computed to estimate coherent synchronized fluctuations in water diffusion at baseline between the left M1 and each of the other regions using the time series data (144 data points). Error bars indicate SEM. Correlation was significant when the right PM or left SPL was paired with the left M1 ($P < 0.001$) but not significant when the left PM ($P = 0.15$) or SMA ($P = 0.60$) was paired with the left M1. R^2 was largest between the right PM and the left M1 (right PM vs. left SPL, $P < 0.001$), followed by the left SPL (left SPL vs. left PM, $P < 0.001$) and then the SMA (left PM vs. SMA, $P = 0.007$).

fluctuations in water diffusion were not synchronized with the left M1 (the left PM and the SMA) showed a faster decay in the rTMS-induced change in water diffusion (<10 min), and the magnitude of the rTMS-induced change in water diffusion in the left M1 was not correlated with that in the left PM or the SMA.

The effect of rTMS on water diffusion has been studied in a few previous reports, but their results are inconclusive (26, 27). Previous studies quantified the rTMS-induced change in regional water diffusion in the stimulated M1 relative to the change in a control region on the assumption that rTMS did not affect water diffusion in remote nonstimulated regions (26). However, using voxel-based comparisons between the before and immediately after rTMS time points, our study demonstrated that changes in water diffusion occurred in remote regions and in the stimulated M1, supporting previous neuroimaging studies (7, 8) and suggesting that the effects of rTMS are propagated to remote regions of the brain.

It is notable that baseline fluctuations in water diffusion in the left M1 synchronized with those in the left SPL and right PM (Fig. 4), and these are the regions that retained the altered water diffusion for 10 min after the end of the stimulation (Fig. 3 and Fig. S3). These results suggest that retention occurred due to synchronization of water diffusion between the three regions (Fig. 4 and Fig. S4). On the other hand, baseline fluctuations in water diffusion in the left PM and SMA were not synchronized with those in the left M1, and these regions failed to retain the altered water diffusion for 10 min after the end of the stimulation. These findings suggest the presence of networks that involve the stimulated cortex and remote nonstimulated regions that are relevant to the retention of rTMS effects in remote regions of the brain, and thus are a possible neural substrate for rTMS-induced plasticity in multiple regions. The networks that were revealed by probing water diffusion modulated retention of the rTMS carryover effect in remote regions of the brain, whereas neuronal networks that were identified in previous studies did not (8, 28); therefore, it is possible that the networks identified in our study might functionally differ from previously identified neuronal networks, although the nodal regions of these two networks do overlap (8). This issue requires further investigation.

Recent evidence suggests that synaptic activation, which includes intracellular molecular events, induces an immediate morphological response (29–31) or a delayed LTP/LTD-related change (32–37) in microstructures in neural tissue that can modulate intracortical water diffusion (12, 20) (Fig. S5). The interregional correlation in water diffusion observed before rTMS might reflect synchronization of the activity-dependent fluctuations in the morphology of cortical microstructures between the left M1 and other regions. The increase in water diffusion after rTMS might be a result of decreased density of dendritic spines, as observed in LTD-like plasticity (20). It is also possible that dynamical coupling in the morphology of microstructures allows the formation of networks to represent the plasticity-related morphological changes following brain stimulation protocols. The morphology of dendritic spines can modulate synaptic efficacy and plasticity (3, 4, 38); therefore, it is possible that the nodes in the identified networks can indirectly achieve long-distance coupling with each other by modulating synaptic plasticity or efficacy of the transsynaptic signaling (39).

DWI was developed as a clinical probe to estimate structural changes under pathological conditions that alter intracortical water diffusion (40). Recently, much attention has been paid to this technique because it is a sensitive probe that can be used under physiological conditions to evaluate acute responses associated with neuronal firing (13, 16, 19) and delayed changes that are correlated with molecular processes for the formation of LTP or LTD (20). Our results support a potential use of DWI techniques to estimate plasticity-related changes in nonstimulated remote regions after repetitive brain stimulation. Although further investigations are needed to identify more specific probes of plasticity, DWI techniques could provide a new biomarker to estimate changes in plastic microstructure in neural tissue that occur following repetitive brain stimulation protocols or epilepsy.

In conclusion, a 10-min-long period of subthreshold 1-Hz rTMS produced LTD-like plasticity in the left M1 and a multiregional increase in water diffusion in the left M1, left PM, left SPL, right PM, and SMA immediately after the end of the stimulation. At rest, water diffusion in left SPL and right PM was synchronized with water diffusion in the left M1, and this permitted retention of rTMS-induced increases in water diffusion for 10 min after the end of rTMS to the left M1. Given that morphological changes related to synaptic activation or plasticity can modulate water diffusion, these results indicate that synchronization of basal fluctuations in the morphology of cortical microstructures between stimulated and remote regions might underlie the formation of plasticity in remote regions after brain stimulation protocols. These results increase our understanding of the effects of brain stimulation-induced plasticity on multiregional brain networks. DWI techniques could provide a tool to evaluate treatment effects of brain stimulation protocols in patients with brain disorders.

Methods

Subjects. Twelve right-handed, healthy young adult volunteers (mean age, 29.3 y; range, 21–40 y) participated in this study. All participants were right-handed as assessed by the Edinburgh Handedness Inventory, had no abnormal physical or neurological findings, no history of neurological or psychiatric diseases, and did not take chronic medications. All subjects gave written informed consent to participate in the study before the experiment. The

study protocol was approved by the Kyoto University Graduate School and Faculty of Medicine Ethics Committee.

Experimental Design. Functional DWI techniques were used to estimate intracortical water diffusion (14, 16). The MRI-compatible TMS and EMG system that was developed by Hanakawa et al. (24) was located inside the bore of an MRI scanner and enabled TMS to be delivered, MEPs to be measured, and MRI to be obtained while the subject's head was inside the bore.

MEPs were measured and DWI was performed during periods of rest before (baseline) and after the repetitive TMS (rTMS; Fig. 1). The subject was instructed not to move his/her head and to gaze at a central fixation point on a projected screen during the entire experiment. Measurements were performed at two baseline time points separated by 10 min, the same length as the rTMS period, to examine the stability of brain water diffusion without rTMS. Subthreshold, low-frequency rTMS was then applied to hand area of the left M1 for 10 min. Measurements were performed at three poststimulation time points: immediately and 10 and 20 min after rTMS.

Electrophysiological Measurements. A figure-eight-shaped TMS coil with an outer-wing diameter of 70 mm (MR coil; Magstim) was used throughout the experiment. The location on the scalp at which TMS evoked maximal amplitude of MEPs in the right abductor pollicis brevis muscle (the motor hotspot) was identified and marked for each subject while they were sitting comfortably on a chair outside the scanner. The subject then lay supine on the bed of a 3-T MRI scanner (Siemens Magnetom Trio). Surface EMG electrodes were placed over the right thenar eminence, and the TMS coil was positioned tangentially to the scalp at the marked site and adjusted to produce the maximal amplitude of MEPs in the right abductor pollicis brevis muscle. The subject's head was positioned inside the bore of the scanner, and resting motor threshold was measured in the right abductor pollicis brevis muscle using the same procedure as described previously (22, 23). For rTMS, a single train of 600 TMS pulses was applied at a frequency of 1.0 Hz and an intensity of 90% of resting motor threshold, and EMG was recorded to monitor the absence of evoked motor responses. Subthreshold stimulation was chosen to minimize the influence of afferent information related to the evoked motor responses on brain activity. At each measurement time point, 20 stimuli were applied at a frequency of 0.1 Hz (i.e., one stimulation every 10 s) and at an intensity of 120% of resting motor threshold (22, 23), and MEPs were monitored in the in the right abductor pollicis brevis muscle.

Image Acquisition. rTMS of the left M1 affects motor-related regions of the brain (7, 8, 41–46); therefore, we acquired images covering these regions with an axial field of view of 40 mm from the top of the brain surface. DWI was performed with a twice refocused spin-echo echo-planar imaging sequence sensitized to diffusion by an interleaved pair of bipolar magnetic field gradient pulses (16). High and low b-value images (b = 1,200 and 300 s/mm^2, respectively) were acquired to estimate mean water diffusion. The high b value was 1,200 s/mm^2 because our preliminary experiment revealed that 1,200 s/mm^2 was the highest b value that could acquire DWI signals with maximized signal-to-noise ratio when using the one-channel MRI coil, which allows the TMS coil to approach the scalp surface from the top (42, 45). Gradient pulses were applied along a single direction (x, y, z = 1, 1, 1), because DWI signals in one sampled direction can be used to estimate mean diffusivity in cortices, on the assumption that water diffusion is not anisotropic within cortical tissue (12). Acquisition parameters were as follows: slice thickness = 2.0 mm with no gap, pixel size = 2.0 × 2.0 mm^2, echo time = 85 ms, repetition time = 3 s, bandwidth = 1,302 Hz. At each time point, a single run of 18 repetitions of four consecutive scans with b = 1,200 s/mm^2 followed by one scan with b = 300 s/mm^2 (i.e., four scans of b1200 DWI alternated with one scan of b300 DWI) were performed. A total of 72 scans of b1200 DWI and 18 scans of b300 DWI were acquired per time point. A high-resolution image of the structural anatomy was also obtained using a 3D magnetization-prepared rapid gradient-echo T1-weighted sequence with the following parameters: slice thickness = 0.95 mm with no gap, pixel size = 0.95 × 0.95 mm^2, echo time = 73 ms, repetition time = 2 s, flip angle = 8°, bandwidth = 130 Hz. This image was used for registration purposes.

Data Analysis. DWI data acquired with a b value of 1,200 s/mm^2 (b1200 DWI data) were used to estimate mean water diffusion because they were more sensitive to changes in intracortical water diffusion than DWI data acquired with a b value of 300 s/mm^2 (14, 16). Previously, we presented the analysis of mean or time-series b1200 DWI data at each time point. The analysis of b300 DWI data and the apparent diffusion coefficient, the index to evaluate water diffusion, are presented in Figs. S2 and S3.

DWI data were first preprocessed for each subject using SPM2 software (Wellcome Department of Cognitive Neuroscience, University College London). Data were corrected for motion across time points and registered to the high-resolution anatomical image. For registration, structural images were spatially normalized to the T1 template, and the DWI data were spatially normalized to the normalized anatomical image for each subject. The normalized data were temporally low-pass filtered to retain frequencies below 0.1 Hz and then spatially smoothed with a Gaussian filter (6 mm full-width-at-half-maximum). The b1200 DWI data and the b300 DWI data were preprocessed in the same manner.

Voxel-based analyses were performed using statistical parametric maps. Mean DWI maps were computed as the average of the 72 images acquired at each time point and were compared between the two baseline time points to evaluate the stability of water diffusion over a 10-min period. The baseline images were averaged across the two baseline time points, and this average was compared with the immediately after rTMS time point to identify the regions with a change in water diffusion immediately after the end of rTMS. The level of significance was set to a cluster of corrected FWE $P < 0.05$. To evaluate the post-rTMS changes over time, comparisons were also performed between the baseline and the 10- and 20-min after rTMS time points and between the immediately and 10-min after rTMS time points. Voxels within a 10-mm sphere centered at the coordinates of the peak signal intensity within the region of interest (Table 1) were tested. Significance was set to a FWE $P < 0.05$ corrected within the search volume of interest. Fig. 3 and Fig. S2 show the signal intensity after normalization for each subject to minimize intersubject variance in the raw signal data. Data were normalized to the raw signal intensity in the first scan of the first baseline time point and then averaged within each time point, as described previously (26).

We also performed region-of-interest analyses to test whether intrinsic fluctuations in water diffusion at baseline were correlated between the left M1 and remote regions (Fig. 4). Water diffusion data were extracted from the b1200 DWI maps and averaged across the voxels within a 10-mm sphere centered at the coordinates of the peak signal intensity within the region of interest (Table 1). The signal intensity was stable across the two baseline measurements; therefore, the 72 data points from each baseline measurement were transformed to a z score and then combined for the regression analyses. The R^2 of the relation between the left M1 and each other region was calculated using the 144 data points from the two baseline measurements. For the bootstrap procedure, an empirical null distribution of the computed R^2 was constructed by replacing the time series bins, which consisted of six data points in each region or across different regions, in a pseudorandom manner from the set of 144 data points (47). Significant coherent correlations with median R^2 significantly greater than the median R^2 of the null distribution (Fig. 4) were identified using a Mann-Whitney U test. Significance was set to a FWE $P < 0.05$ corrected for multiple comparisons. The change in R^2 between the baseline and each post-rTMS time point was examined, and no significant results were found ($P > 0.5$).

ACKNOWLEDGMENTS. We thank Dr. Shin-ichi Urayama for technical support in the initial experimental setup and Drs. Denis Le Bihan, Hartwig R. Siebner, Nobukatsu Sawamoto, and Toyomi Abe for insightful comments on earlier versions of this manuscript. This work was supported by a Takeda Science Foundation grant and partially by a Translational Medical Center Young Investigator Fellowship grant from the National Center of Neurology and Psychiatry (to M.A.); a Grant-in-Aid for Scientific Research (B) 24300192 and a grant for Exploratory Research (24650226) from the Japan Society for the Promotion of Science (to T.M.); and a Grant-in-Aid for Scientific Research (B) 24390292 and a Grant-in-Aid for Scientific Research on Priority Areas (25117008) (to H.F.).

1. Filosa A, et al. (2009) Neuron-glia communication via EphA4/ephrin-A3 modulates LTP through glial glutamate transport. *Nat Neurosci* 12(10):1285–1292.
2. Pannasch U, et al. (2011) Astroglial networks scale synaptic activity and plasticity. *Proc Natl Acad Sci USA* 108(20):8467–8472.
3. Skucas VA, et al. (2011) Impairment of select forms of spatial memory and neurotrophin-dependent synaptic plasticity by deletion of glial aquaporin-4. *J Neurosci* 31(17):6392–6397.
4. Li YK, et al. (2012) Aquaporin-4 deficiency impairs synaptic plasticity and associative fear memory in the lateral amygdala: Involvement of downregulation of glutamate transporter-1 expression. *Neuropsychopharmacology* 37(8):1867–1878.
5. Hallett M, Chokroverty S (2005) *Magnetic Stimulation in Clinical Neurophysiology* (Elsevier Butterworth–Heinemann, Philadelphia), 2nd Ed.
6. Wassermann EM, et al. (2008) *The Oxford Handbook of Transcranial Stimulation* (Oxford Univ Press, Oxford).

7. Okabe S, et al. (2003) Functional connectivity revealed by single-photon emission computed tomography (SPECT) during repetitive transcranial magnetic stimulation (rTMS) of the motor cortex. *Clin Neurophysiol* 114(3):450–457.
8. Siebner HR, et al. (2000) Lasting cortical activation after repetitive TMS of the motor cortex: A glucose metabolic study. *Neurology* 54(4):956–963.
9. George MS, Taylor JJ, Short EB (2013) The expanding evidence base for rTMS treatment of depression. *Curr Opin Psychiatry* 26(1):13–18.
10. Najib U, Bashir S, Edwards D, Rotenberg A, Pascual-Leone A (2011) Transcranial brain stimulation: Clinical applications and future directions. *Neurosurg Clin N Am* 22(2): 233–251, ix.
11. Reis J, et al. (2009) Noninvasive cortical stimulation enhances motor skill acquisition over multiple days through an effect on consolidation. *Proc Natl Acad Sci USA* 106(5): 1590–1595.
12. Le Bihan D (2003) Looking into the functional architecture of the brain with diffusion MRI. *Nat Rev Neurosci* 4(6):469–480.
13. Darquié A, Poline JB, Poupon C, Saint-Jalmes H, Le Bihan D (2001) Transient decrease in water diffusion observed in human occipital cortex during visual stimulation. *Proc Natl Acad Sci USA* 98(16):9391–9395.
14. Flint J, Hansen B, Vestergaard-Poulsen P, Blackband SJ (2009) Diffusion weighted magnetic resonance imaging of neuronal activity in the hippocampal slice model. *Neuroimage* 46(2):411–418.
15. Kimiwada T, et al. (2006) Hippocampal and thalamic diffusion abnormalities in children with temporal lobe epilepsy. *Epilepsia* 47(1):167–175.
16. Le Bihan D, Urayama S, Aso T, Hanakawa T, Fukuyama H (2006) Direct and fast detection of neuronal activation in the human brain with diffusion MRI. *Proc Natl Acad Sci USA* 103(21):8263–8268.
17. Meng S, et al. (2004) Correspondence of AQP4 expression and hypoxic-ischaemic brain oedema monitored by magnetic resonance imaging in the immature and juvenile rat. *Eur J Neurosci* 19(8):2261–2269.
18. Tourdias T, et al. (2009) Aquaporin 4 correlates with apparent diffusion coefficient and hydrocephalus severity in the rat brain: A combined MRI-histological study. *Neuroimage* 47(2):659–666.
19. Tsurugizawa T, Ciobanu L, Le Bihan D (2013) Water diffusion in brain cortex closely tracks underlying neuronal activity. *Proc Natl Acad Sci USA* 110(28):11636–11641.
20. Sagi Y, et al. (2012) Learning in the fast lane: New insights into neuroplasticity. *Neuron* 73(6):1195–1203.
21. Konermann S, et al. (2003) Presurgical evaluation of epilepsy by brain diffusion: MR-detected effects of flumazenil on the epileptogenic focus. *Epilepsia* 44(3):399–407.
22. Chen R, et al. (1997) Depression of motor cortex excitability by low-frequency transcranial magnetic stimulation. *Neurology* 48(5):1398–1403.
23. Romero JR, Anschel D, Sparing R, Gangitano M, Pascual-Leone A (2002) Subthreshold low frequency repetitive transcranial magnetic stimulation selectively decreases facilitation in the motor cortex. *Clin Neurophysiol* 113(1):101–107.
24. Hanakawa T, et al. (2009) Stimulus-response profile during single-pulse transcranial magnetic stimulation to the primary motor cortex. *Cereb Cortex* 19(11):2605–2615.
25. Groppa S, et al. (2012) A practical guide to diagnostic transcranial magnetic stimulation: Report of an IFCN committee. *Clin Neurophysiol* 123(5):858–882.
26. Mottaghy FM, et al. (2003) Repetitive TMS temporarily alters brain diffusion. *Neurology* 60(9):1539–1541.
27. Duning T, et al. (2004) Repetitive TMS temporarily alters brain diffusion. *Neurology* 62(11):2144, author reply 2144–2145.
28. Lee L, et al. (2003) Acute remapping within the motor system induced by low-frequency repetitive transcranial magnetic stimulation. *J Neurosci* 23(12):5308–5318.
29. Fischer M, Kaech S, Knutti D, Matus A (1998) Rapid actin-based plasticity in dendritic spines. *Neuron* 20(5):847–854.
30. McKinney RA (2010) Excitatory amino acid involvement in dendritic spine formation, maintenance and remodelling. *J Physiol* 588(Pt 1):107–116.
31. Testa I, et al. (2012) Nanoscopy of living brain slices with low light levels. *Neuron* 75(6):992–1000.
32. Monfils MH, Teskey GC (2004) Induction of long-term depression is associated with decreased dendritic length and spine density in layers III and V of sensorimotor neocortex. *Synapse* 53(2):114–121.
33. Nägerl UV, Eberhorn N, Cambridge SB, Bonhoeffer T (2004) Bidirectional activity-dependent morphological plasticity in hippocampal neurons. *Neuron* 44(5):759–767.
34. Zhou Q, Homma KJ, Poo MM (2004) Shrinkage of dendritic spines associated with long-term depression of hippocampal synapses. *Neuron* 44(5):749–757.
35. Wang XB, Yang Y, Zhou Q (2007) Independent expression of synaptic and morphological plasticity associated with long-term depression. *J Neurosci* 27(45):12419–12429.
36. Bastrikova N, Gardner GA, Reece JM, Jeromin A, Dudek SM (2008) Synapse elimination accompanies functional plasticity in hippocampal neurons. *Proc Natl Acad Sci USA* 105(8):3123–3127.
37. Wosiski-Kuhn M, Stranahan AM (2012) Transient increases in dendritic spine density contribute to dentate gyrus long-term potentiation. *Synapse* 66(7):661–664.
38. Scharfman HE, Binder DK (2013) Aquaporin-4 water channels and synaptic plasticity in the hippocampus. *Neurochem Int* 63(7):702–711.
39. Pereira A, Jr., Furlan FA (2010) Astrocytes and human cognition: Modeling information integration and modulation of neuronal activity. *Prog Neurobiol* 92(3): 405–420.
40. Kloska SP, Wintermark M, Engelhorn T, Fiebach JB (2010) Acute stroke magnetic resonance imaging: Current status and future perspective. *Neuroradiology* 52(3): 189–201.
41. Baudewig J, et al. (2001) Functional MRI of cortical activations induced by transcranial magnetic stimulation (TMS). *Neuroreport* 12(16):3543–3548.
42. Bestmann S, Baudewig J, Siebner HR, Rothwell JC, Frahm J (2003) Subthreshold high-frequency TMS of human primary motor cortex modulates interconnected frontal motor areas as detected by interleaved fMRI-TMS. *Neuroimage* 20(3):1685–1696.
43. Chouinard PA, Van Der Werf YD, Leonard G, Paus T (2003) Modulating neural networks with transcranial magnetic stimulation applied over the dorsal premotor and primary motor cortices. *J Neurophysiol* 90(2):1071–1083.
44. Speer AM, et al. (2003) Intensity-dependent regional cerebral blood flow during 1-Hz repetitive transcranial magnetic stimulation (rTMS) in healthy volunteers studied with H215O positron emission tomography: I. Effects of primary motor cortex rTMS. *Biol Psychiatry* 54(8):818–825.
45. Bestmann S, Baudewig J, Siebner HR, Rothwell JC, Frahm J (2004) Functional MRI of the immediate impact of transcranial magnetic stimulation on cortical and subcortical motor circuits. *Eur J Neurosci* 19(7):1950–1962.
46. Cárdenas-Morales L, Grön G, Kammer T (2011) Exploring the after-effects of theta burst magnetic stimulation on the human motor cortex: A functional imaging study. *Hum Brain Mapp* 32(11):1948–1960.
47. Roebroeck A, Formisano E, Goebel R (2005) Mapping directed influence over the brain using Granger causality and fMRI. *Neuroimage* 25(1):230–242.